Ya Ge
School of Energy and Power Engineering,
Huazhong University of Science and Technology,
1037 Luoyu Road,
Wuhan 430074, China
e-mail: geya@hust.edu.cn

Feng Shan
School of Energy and Power Engineering,
Huazhong University of Science and Technology,
1037 Luoyu Road,
Wuhan 430074, China
e-mail: shanfeng@hust.edu.cn

Zhichun Liu[1]
School of Energy and Power Engineering,
Huazhong University of Science and Technology,
1037 Luoyu Road,
Wuhan 430074, China
e-mail: zcliu@hust.edu.cn

Wei Liu
School of Energy and Power Engineering,
Huazhong University of Science and Technology,
1037 Luoyu Road,
Wuhan 430074, China
e-mail: w_liu@hust.edu.cn

Optimal Structural Design of a Heat Sink With Laminar Single-Phase Flow Using Computational Fluid Dynamics-Based Multi-Objective Genetic Algorithm

This paper proposes a general method combining evolutionary algorithm and decision-making technique to optimize the structure of a minichannel heat sink (MCHS). Two conflicting objectives, the thermal resistance θ and the pumping power P, are simultaneously considered to assess the performance of the MCHS. In order to achieve the ultimate optimal design, multi-objective genetic algorithm is employed to obtain the nondominated solutions (Pareto solutions), while technique for order preference by similarity to an ideal solution (TOPSIS) is employed to determine which is the best compromise solution. Meanwhile, both the material cost and volumetric flow rate are fixed where this nonlinear problem is solved by applying the penalty function. The results show that θ of Pareto solutions varies from 0.03707 K W^{-1} to 0.10742 K W^{-1}, while P varies from 0.00307 W to 0.05388 W, respectively. After the TOPSIS selection, it is found that P is significantly reduced without increasing too much θ. As a result, θ and P of the optimal MCHS determined by TOPSIS are 35.82% and 52.55% lower than initial one, respectively.
[DOI: 10.1115/1.4037643]

Introduction

With the rapid development of the microfabrication technologies, the increasing heat generation makes a proper thermal management solution critical to the electronic devices. In the beginning of the 1980s, Tuckerman and Pease [1] first proposed the micro/minichannel heat sink (MCHS) and found it was able to dissipate a heat flux of 790 W cm^{-2}. Subsequently, considerable experimental, analytical and numerical studies have been made to improve the performance. Samalam [2] theoretically studied the MCHS and described the correlations for thermal resistance. By employing the finite volume method, Xie et al. [3] found that pressure drop and thermal resistance varied with the channel height, width, wall thickness, and bottom plate thickness. Wan et al. [4] made an experimental analysis of flow and heat transfer in a miniature porous heat sink. Persoons et al. [5] investigated the effect of flow pulsation of a minichannel heat sink.

When optimizing a heat transfer unit or a system, the flow resistance often has an increase with the enhancement of heat transfer [6–10]. In general, the micro/minichannel offers a large heat transfer area and a high convective heat transfer coefficient, while high pumping power is also required for driving the fluid. Therefore, evaluation criteria, such as performance evaluation criteria [11] and JF (Colburn j and friction f factors) factor [12], play a significant role in assessing the comprehensive performance or economic benefit of MCHS. However, it is sometimes inconvenient to choose a proper evaluation criterion since different evaluation criteria conflict with each other. Recently, multi-objective optimization techniques have received more and more attention in many fields [13–15]. Different from the existing evaluation criteria that combine several objective functions into a single objective function, multi-objective optimization involves more than one objective function to be optimized simultaneously. Copiello and Fabbri [16] coupled a simplified numerical method and the strength Pareto evolutionary algorithm 2 to optimize longitudinal wavy fins. Husain and Kim [17] used a fast and elitist nondominated sorting genetic algorithm in order to determine three optimal nondimensional geometry variables of a liquid flow microchannel heat sink. Abdoli and Dulikravich [18] applied response surface approximation and genetic algorithm in order to achieve three objectives: maximizing amount of heat removed, minimizing temperature nonuniformity on hot surface, and minimizing viscous losses.

In the present work, a minichannel heat sink has been optimized by means of a multi-objective genetic algorithm where the two objectives are the minimization of the thermal resistance (θ) and, at the same time, the minimization of the pumping power (P). Instead of simplified numerical models or surrogate models mainly applied in the existing literature, a three-dimensional numerical model is optimized here by coupling the finite element method and genetic algorithm [19]. After the optimization, the initial population converges to a set of nondominated solutions, called the Pareto front. Subsequently, a decision-making technique, technique for order preference by similarity to an ideal solution (TOPSIS) [20], is employed to determine the compromise solution from the Pareto front. Furthermore, the material cost and volumetric flow rate are fixed where the penalty function is applied to solve this nonlinear problem.

Problem Description

Model and Governing Equations. The schematic of minichannel is shown in Fig. 1. The heat is supplied from the bottom with dimensions of $W \times L$ and transferred to the channels with dimensions of $W_c \times L \times H_c$. Subsequently, the cooling water which is forced to flow through the channels removes the heat conducted through the solid. The bottom plate thickness is H_b, and the channel wall thickness is W_w. The top lid thickness is not

[1]Corresponding author.

Contributed by the Heat Transfer Division of ASME for publication in the Journal of Heat Transfer. Manuscript received September 24, 2016; final manuscript received June 29, 2017; published online September 26, 2017. Assoc. Editor: Amitabh Narain.

included and regarded as the adiabatic wall. In the present study, parameters of the initial MCHS are $W_w = W_c = 0.5$ mm, $H_c = 2$ mm, and $H_b = 1$ mm, with $u_{in} = 1$ m s^{-1}.

Figure 2 illustrates the cross section of the computational domain of the minichannel. A no-slip condition is applied at the interior walls. In order to save the computing time, symmetric boundary conditions are applied in the present work. Moreover, the following assumptions are made in the numerical simulations:

(1) The water flow is three-dimensional, laminar, incompressible, and in steady-state.
(2) All the thermophysical properties are constant and the heat flux is uniform.
(3) The gravitational force is neglected.

Based on the above assumptions, the governing equations including the continuity, momentum, and energy can be expressed as follows.

Continuity equation for the coolant:

$$\nabla \cdot \mathbf{V} = 0 \tag{1}$$

Momentum equation for the coolant:

$$\rho_f(\mathbf{V} \cdot \nabla \mathbf{V}) = -\nabla p + \nabla \cdot (\mu_f \nabla \mathbf{V}) \tag{2}$$

Energy equation for the coolant:

$$\rho_f c_{p,f}(\mathbf{V} \cdot \nabla T) = \lambda_f \nabla^2 T \tag{3}$$

Energy equation for the solid:

$$\lambda_s \nabla^2 T = 0 \tag{4}$$

Other boundary conditions needed for the computational unit are listed as follows [21,22]:

at $x = 0$, $W_w/2 \le y \le (W_w + W_c)/2$ and $H_b \le z \le H_b + H_c$:

$$u = u_{in},\ v = w = 0,\ T = T_{in} \tag{5}$$

at $x = L$, $W_w/2 \le y \le (W_w + W_c)/2$ and $H_b \le z \le H_b + H_c$:

$$\frac{\partial u}{\partial x} = \frac{\partial v}{\partial x} = \frac{\partial w}{\partial x} = 0,\ p = p_{out} \tag{6}$$

at $z = 0$

$$-\lambda_s \frac{\partial T}{\partial z} = q \tag{7}$$

at $z = H_b + H_c$

$$\frac{\partial T}{\partial z} = 0 \tag{8}$$

In this study, the above governing equations along with the boundary conditions are solved by a finite element software, COMSOL MULTIPHYSICS. T_{in} is 300 K and q is 100 W cm^{-2}. In each case of the simulation, the flow and thermal field are computed with approximately 200,000 degrees-of-freedom. All the simulations are done on a workstation with two eight-core CPUs (E5-2670) and 64 GB RAM. Under such conditions, it takes approximately 3 min to complete a single case and 250 h to complete an entire multi-objective optimization procedure.

Objective Functions. Instead of using a combined objective function, the multi-objective method considers all the design requirements simultaneously. In this paper, two conflicting objective functions are defined as follows:

$$J_1 = \theta, \quad J_2 = P \tag{9}$$

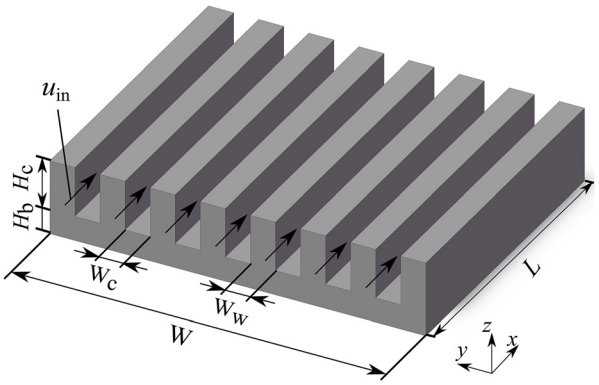

Fig. 1 Schematic diagrams of MCHS

As mentioned earlier, thermal resistance θ is calculated to assess the performance of heat transfer, while pumping power P is calculated to assess the performance of flow resistance, respectively. The thermal resistance can be calculated from

$$\theta = \frac{T_{max} - T_{in}}{q \times N \times (W_c + W_w) \times L} \tag{10}$$

where T_{max} is the maximum temperature at the base, N is the number of channel, which equals to the integer part of $W/(W_c + W_w)$. The initial MCHS width W and length L are 20 mm, respectively. Besides, it is noticed that the optimal MCHS width W' may vary as channel unit geometry alters, which is also considered in the present work.

On the other hand, the pumping power is expressed as

$$P = \dot{V} \times \Delta p \tag{11}$$

where $\dot{V}$ is the volumetric flow rate of MCHS and Δp is the pressure drop through the channel.

Therefore, an optimal heat sink with low flow resistance and high heat transfer coefficient can be achieved as J_1 and J_2 are approaching minimum values. However, it is worth noting that the results of the multi-objective optimization are not a unique optimal solution but a set of nondominant solutions. The entire optimization procedure including the selecting technique is described in the Optimization Procedure section.

Optimization Procedure

Multi-Objective Optimization Algorithm. For many complex engineering problems, objectives under consideration often

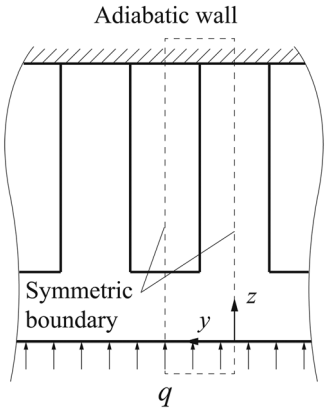

Fig. 2 Computational domain

conflict with each other. When multiple objectives are involved, there is a common phenomenon that all the objective functions are combined into a single composite objective function for evaluating the overall performance, such as utility theory and weighted sum method. There are some inherent limitations since defining the weights is a difficult issue and some evaluation criteria also conflict with each other. The multi-objective evolutionary algorithms, however, are generalized approaches to determine a set of nondominant solutions (Pareto solutions). In the present study, an efficient multi-objective evolutionary algorithm, the nondominated sorting genetic algorithm [23], is employed to optimize two objective functions defined earlier. Following the concept of this algorithm, all individuals are ranked according to their fitness score based on the objective function values. Subsequently, in the process of selection, fitter solutions with high fitness score are more likely to be selected and preserved. Therefore, as the iterative process continues, the Pareto optimal solutions will be evolved gradually.

TOPSIS Selection. After obtaining the Pareto front consisting of Pareto solutions, the next step is to determine the best compromise solution for the application. Generally, selection work in multi-objective optimization is much more complex since each Pareto solution represents a compromise solution under different objective functions and we cannot directly choose the best one. However, following the basic concept that the chosen alternative should have the shortest distance from the positive ideal solution and the longest distance from the negative ideal solution, TOPSIS is a practical and classical approach for ranking and selecting alternatives. In this design work, the positive ideal solution has the smallest thermal resistance and pumping power, and the negative ideal solution is just the opposite. The computational procedure of TOPSIS is as follows:

(1) Create a matrix $(x_{ij})_{m\times n}$ with m alternatives and n objectives.
(2) Normalize the matrix $(x_{ij})_{m\times n}$ to $(t_{ij})_{m\times n}$ by using the equation below:

$$t_{ij} = \frac{x_{ij}}{\sqrt{\sum_{i=1}^{m} x_{ij}^2}}, i = 1, 2, ..., m, j = 1, 2, ..., n \tag{12}$$

(3) Set the weight coefficient w_j and obtain the weighted normalized matrix $(a_{ij})_{m\times n}$ by

$$a_{ij} = w_j \times t_{ij}, i = 1, 2, ..., m, j = 1, 2, ..., n \tag{13}$$

(4) Determine the positive ideal alternative A^+ and the negative ideal alternative A^-

$$A^+ = (\min[a_{11}, ...a_{m1}], \min[a_{12}, ...a_{m2}], ..., \min[a_{1n}, ...a_{mn}]) \tag{14}$$

$$A^- = (\max[a_{11}, ...a_{m1}], \max[a_{12}, ...a_{m2}], ..., \max[a_{1n}, ...a_{mn}]) \tag{15}$$

(5) Calculate the distance between the target alternative A and the positive ideal alternative A^+, and the distance between the target alternative A and the negative ideal alternative A^-:

$$d_i^+ = \sqrt{\sum_{j=1}^{n} (a_{ij} - A_j^+)^2}, i = 1, 2, ..., m, j = 1, 2, ..., n \tag{16}$$

$$d_i^- = \sqrt{\sum_{j=1}^{n} (a_{ij} - A_j^-)^2}, i = 1, 2, ..., m, j = 1, 2, ..., n \tag{17}$$

(6) Calculate the relative closeness to the ideal solution of alternatives

$$C_i = \frac{d_i^-}{d_i^+ + d_i^-}, i = 1, 2, ..., m \tag{18}$$

(7) Rank the alternatives according to the values of C_i, and the final compromise solution A_{final} is

$$A_{\text{final}} = A \in \max(C_i) \tag{19}$$

Constraints and Design Variables. For the purpose of application and fabrication, some constraints are considered in the present optimization work

(1) The volumetric flow rate is fixed.
(2) The materials cost of MCHS is constant (i.e., the volume of copper is fixed).

The mathematical form is

$$(N \times u_{\text{in}} \times W_{\text{c}} \times H_{\text{c}})_i = \text{constant} \tag{20}$$

$$(H_{\text{b}} \times N \times (W_{\text{c}} + W_{\text{w}}) + N \times W_{\text{w}} \times H_{\text{c}})_i = \text{constant} \tag{21}$$

The next step is determining the design variables which will affect the comprehensive performance. Xie et al. [3] investigated the influence of channel height H_{c}, channel width W_{w}, wall thickness W_{c}, and bottom plate thickness H_{b}. Based on their results, H_{c}, W_{c}, and W_{w} are selected as design variables while H_{b} can be obtained by Eq. (21). The design variables for the optimization of the present heat sink configurations are allowed to vary within the following ranges:

$$\begin{gathered} 2\,\text{mm} \le H_{\text{c}} \le 4\,\text{mm} \\ 0.2\,\text{mm} \le W_{\text{w}} \le 0.8\,\text{mm} \\ 0.2\,\text{mm} \le W_{\text{c}} \le 0.8\,\text{mm} \end{gathered} \tag{22}$$

Moreover, $H_{\text{b}} \ge 0.2$ mm is also considered for ease of manufacture. From Eq. (21), it is obvious that this constraint is nonlinear. In the present study, the penalty function based on the concept of genetic algorithm is applied to solve this problem. This method replaces a constrained optimization problem by several of unconstrained problems. To be specific, infeasible solutions (i.e., $H_{\text{b}} < 0.2$ mm) are also allowed into the population but the fitness values are modified according to the penalty function. After sufficient time, the optimal solutions to the unconstrained problem using the modified fitness values coincide with those of the original constrained problem. The entire optimization procedure is shown in Fig. 3.

Results and Discussion

Validation. In the COMSOL MULTIPHYSICS, the solution time and memory requirements are strongly related to the number of degrees-of-freedom which depend on the meshing type, the shape functions selected, and the number of dependent variables from the different physics. Due to the simple geometry of the MCHS, the hexahedral grid is constructed for the present numerical simulation. Subsequently, three different grid schemes with different numbers of degrees-of-freedom are tested to guarantee that the simulation results are independent on the grid, which is listed in Table 1. It is found that the max error for this study between grid 2 and grid 3 is 1.8281%. However, the computation time of grid 3 is about twice that of grid 2. Hence, grid 2 is applied in the optimization to improve computation efficiency without loss in accuracy.

In order to provide a numerical validation, the results of the present work are compared with the previous work proposed by Xie et al. [3]. As shown in Figs. 4 and 5, both thermal resistance θ and pressure drop Δp decrease as H_{c} increases, which is in good agreement with the reference. When H_{c} varies from 2 mm to

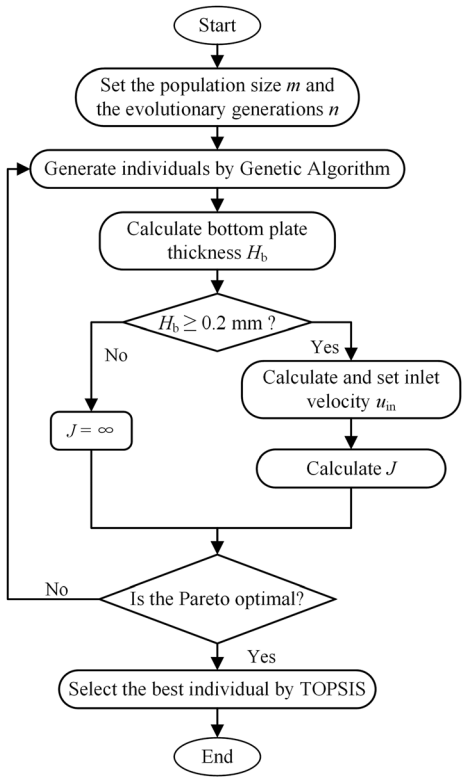

Fig. 3 Flowchart of the optimization work

4 mm, the maximum differences of θ and Δp are 8.11% and 3.54%, respectively. Therefore, the cases used in the present study are valid for optimization work.

Multi-Objective Optimization Results. Figure 6 illustrates the Pareto front obtained by using the proposed design method. It is obvious that the pumping power P would not decrease from one Pareto optimal to another except increasing the thermal resistance θ, which means all these solutions obtained are nondominated. Besides, it is found that P varies from 0.00307 W to 0.05388 W and θ varies from 0.03707 K W^{-1} to 0.10742 K W^{-1}.

Figure 7 gives optimal parameters of the heat sink from the Pareto front. The individual numbers are sorted by ascending the values of θ. It is found that the values of optimal W_w are basically unchanged in the range from 0.2073 mm to 0.2422 mm. Similarly, the optimal values of H_c are also basically unchanged around 3.9 mm when the individual number of Pareto front greater than 10 (i.e., $P < 0.033$ W). The above results indicate that MCHS with higher H_c and lower W_w may have a better comprehensive performance in the present study. On the other hand, W_c and H_b gradually increase along with the entire Pareto front. Besides, it is noticed that H_b is in the range from 0.2066 mm to 1.1730 mm, which satisfies the condition of $H_b \geq 0.2$ mm. Based on this result, it is proved that the penalty function can effectively solve the nonlinear problem in this study.

Table 1 Grid-independent test with $H_c = 2$ mm, $W_c = 0.5$ mm, $W_w = 0.5$ mm, $H_b = 1$ mm, and $u_{in} = 1$m s^{-1}

	Degrees-of-freedom	θ (K W^{-1})	% error	P (W)	% error
Grid 1	86,893	0.09001	1.1422	0.02437	3.4469
Grid 2	181,195	0.09105	0.5461	0.02524	1.8281
Grid 3	347,680	0.09155	—	0.02571	—

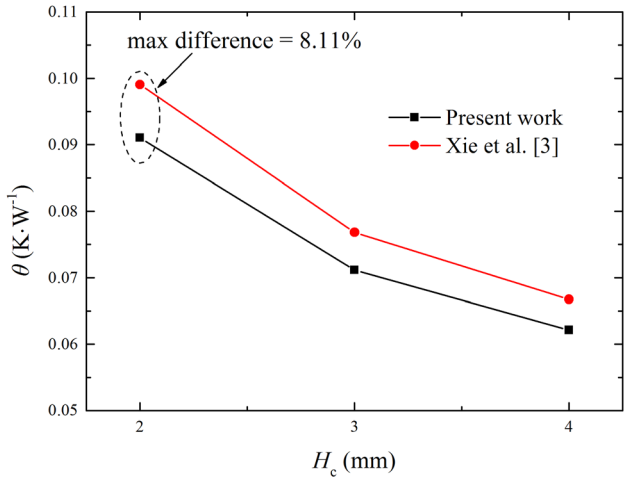

Fig. 4 Comparison of present thermal resistance, θ, with previous work obtained by Xie et al. [3], for $W_w = W_c = 0.5$ mm, $H_b = 1$ mm, and $u_{in} = 1$ m s^{-1}

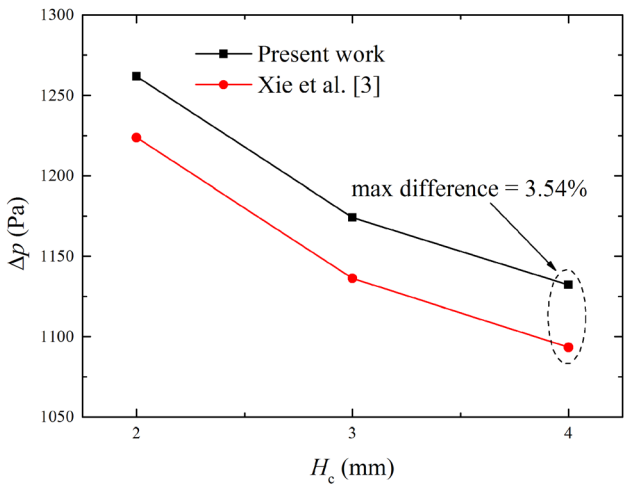

Fig. 5 Comparison of present pressure drop, Δp, with previous work obtained by Xie et al. [3], for $W_w = W_c = 0.5$ mm, $H_b = 1$ mm, and $u_{in} = 1$ m s^{-1}

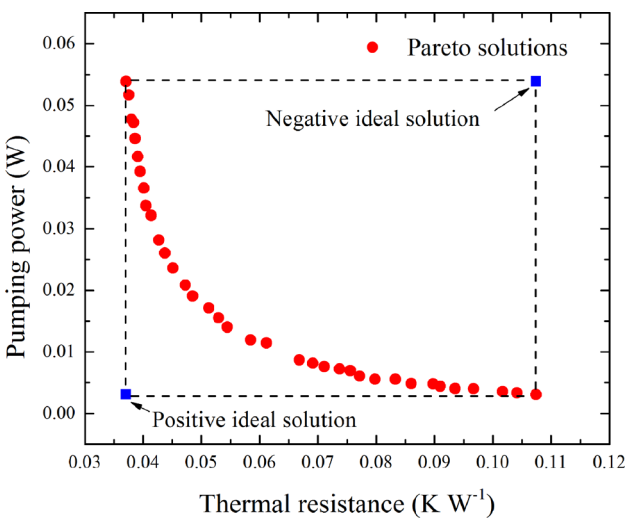

Fig. 6 Distribution of the Pareto front

Other information of minichannel unit, including inlet velocity (u_{in}), inlet area (a_{in}), and numbers of channel units (N), is illustrated in Fig. 8. It is found that both u_{in} and N gradually decrease along with the Pareto front, while a_{in} is contrary to them. Furthermore, it is noticed that all the optimal values of u_{in} are less than 1 m s^{-1}, which means the initial inlet velocity is excessively high and not appropriate for the application.

Subsequently, the optimal width W' and hydraulic diameter D_h of whole MCHS are illustrated in Fig. 9. The optimal W' varies from 19.3275 mm to 19.9988 mm, which is 3.363% to 0.006% less than the initial width W. According to the above results, it could be speculated that the additional material will have little influence on both the performance and cost if heat sink width needs to meet the requirement. On the other hand, D_h has a significant increase from 0.3855 mm to 1.3002 mm, since the structure of MCHS keeps changing along with the Pareto front. Furthermore, the fluid flowing situation which is described by the Reynolds number (Re) also alters with u_{in} and D_h. However, it can be found that all the Reynolds numbers are less than 2300, which means the laminar assumption is suitable in this study.

Selection and Comparison. As shown in Fig. 6, all the Pareto solutions are nondominated and we cannot directly choose the best one according to the values of θ or P. Nevertheless, it is noticed that further reduction for θ is much more difficult than early stages, which means the comprehensive performance of solutions at each end of the Pareto front should not be high. In the present study, the best compromise solution is determined by employing TOPSIS previously described, where $w_1 = w_2 = 0.5$. Table 2 gives the scores of Pareto solutions and the 19th individual from the Pareto front is selected as the best compromise solution. Its position on Fig. 6 accords with the concept that the best solution should be close to the ideal positive solution.

In order to investigate the effects of the optimization and selection, performances of different optimal solutions and the initial one are illustrated in Fig. 10. $\theta_{minimum}$ and $P_{minimum}$ represent the optimal solutions with the minimum thermal resistance and minimum pumping power, respectively. Compared with the initial one, the thermal resistance can be reduced by 59.29% with an increase of 113.48% in pumping power, while the pumping power can be reduced by 87.82% with an increase of 17.98% in thermal resistance, respectively. It is indicated that both θ and P can be greatly improved when single-objective optimization is considered.

Figure 10 also shows the effect of decision-making technique on balancing two conflicting objectives, where optimal$_{TOPSIS}$ represents the optimal solution determined by TOPSIS. Comparison between $\theta_{minimum}$ and optimal$_{TOPSIS}$ shows that the thermal resistance of optimal$_{TOPSIS}$ is 57.64% higher than $\theta_{minimum}$, but the pumping power of optimal$_{TOPSIS}$ is 77.77% lower than $\theta_{minimum}$. Similarly, when comparing $P_{minimum}$ and optimal$_{TOPSIS}$, it is found that pumping power of $P_{minimum}$ is 77.77% lower than optimal$_{TOPSIS}$ while thermal resistance has an increase of 83.83%. As a result, using TOPSIS is effective for improving heat transfer performance of MCHS without bringing too much pumping

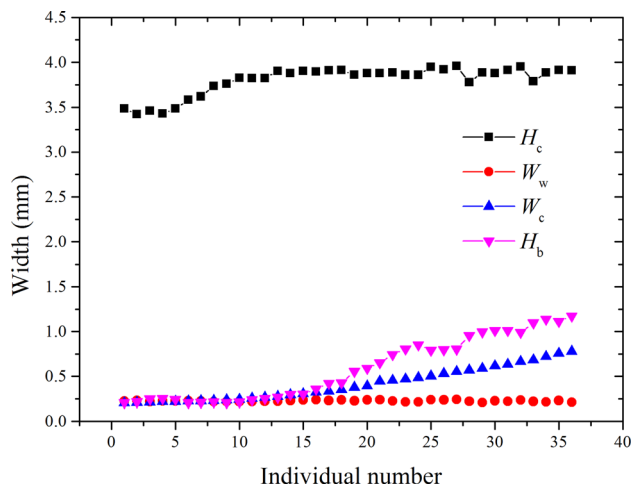

Fig. 7 Variation of four optimal design parameters along with the Pareto front

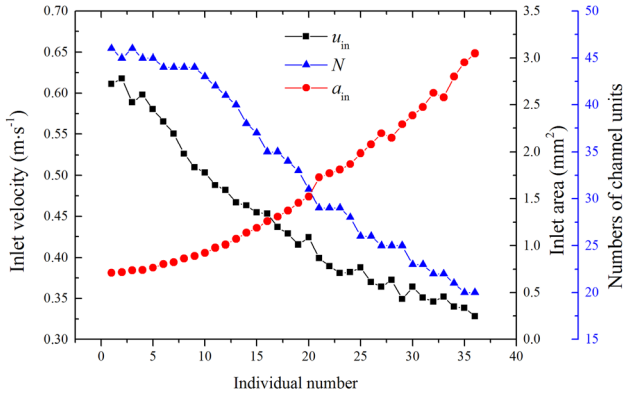

Fig. 8 Variation of inlet velocity, inlet area, and channel numbers along with the Pareto front

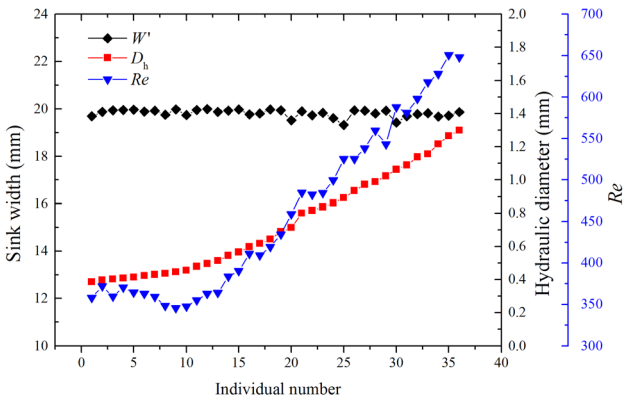

Fig. 9 Variation of heat sink width, hydraulic diameter, and Reynolds number along with the Pareto front

Table 2 Relative closeness and ranking results of the Pareto solutions

Individual#	Score	Rank	Individual#	Score	Rank
1	0.3451	36	19	0.7918	1
2	0.3543	35	20	0.7868	3
3	0.3778	34	21	0.7907	2
4	0.3805	33	22	0.784	4
5	0.4005	32	23	0.7788	5
6	0.4266	31	24	0.7687	7
7	0.4504	30	25	0.7619	8
8	0.48	29	26	0.7597	9
9	0.5143	28	27	0.7504	11
10	0.5325	27	28	0.7348	13
11	0.5857	26	29	0.7265	14
12	0.6147	25	30	0.7112	16
13	0.6495	24	31	0.7081	17
14	0.6887	19	32	0.6997	18
15	0.7141	15	33	0.6878	20
16	0.7387	12	34	0.672	21
17	0.7593	10	35	0.6645	22
18	0.7775	6	36	0.6549	23

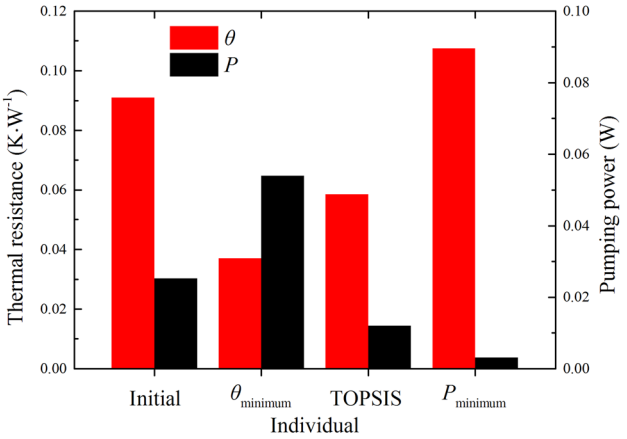

Fig. 10 Performances of the initial and different optimal individuals

power. Furthermore, both θ and P of optimal$_{\text{TOPSIS}}$ are lower (35.82% and 52.55%, respectively) than those of initial one, which demonstrates the effectiveness of the approach proposed in this paper.

Conclusions

The structural design of minichannel heat sink is a multi-objective problem taking minimum thermal resistance and pumping power into consideration, simultaneously. The cost of material and volumetric flow rate are fixed in the present study, where penalty function is applied to solve this nonlinear problem. In the optimization process, multi-objective genetic algorithm and finite element method are coupled to solve the problem mentioned earlier and obtain a series of Pareto solutions. Subsequently, TOPSIS technique is employed to rank these solutions and determine the best compromised one.

Based on the optimization results, the following conclusions can be drawn:

(1) For the optimal solutions, as θ increases and P decreases, W_{w} is basically unchanged in the range from 0.2073 mm to 0.2422 mm, while H_{c} increases from 3.4856 mm and is also basically unchanged when $P < 0.033$ W. On the other hand, W_{c} and H_{b} gradually increase along with the entire Pareto front.

(2) Since the structures have been greatly changed after the optimization, both D_{h} and Re have a significant increase as θ increases, but the flowing situation keeps as laminar. The optimal W' is essentially constant, which means the performance and cost will be almost unaffected if heat sink width needs to meet the requirement.

(3) In the present study, one objective function can be substantially reduced regardless the influence on the other one. After the TOPSIS selection, θ and P have been appropriately balanced. Consequently, both θ and P of optimal$_{\text{TOPSIS}}$ are lower (35.82% and 52.55%, respectively) than those of initial one.

Funding Data

- National Key Basic Research Program of China (973 Program) (Grant No. 2013CB228302).
- National Natural Science Foundation of China (Grant No. 51376069).

Nomenclature

a = area
C = relative closeness to the ideal solution
c_{p} = specific heat
D_{h} = hydraulic diameter
H = height or thickness
J = objective function
L = channel length
p = pressure
P = pumping power
Re = Reynolds number, $\rho_{\text{f}} u_{\text{in}} D_{\text{h}}/\mu_{\text{f}}$
T = temperature
u = flow velocity
V = volumetric flow rate
x, y, z = orthogonal coordinate system
Δp = pressure drop

Greek Symbols

θ = dimensionless temperature
λ = thermal conductivity
μ = dynamic viscosity
ρ = fluid density

Superscripts

b = bottom
c = channel
f = fluid
in = inlet
max = maximum value
s = solid
w = wall

References

[1] Tuckerman, D. B., and Pease, R. F. W., 1981, "High-Performance Heat Sinking for VLSI," IEEE Electron Device Lett., **2**(5), pp. 126–129.
[2] Samalam, V. K., 1989, "Convective Heat Transfer in Microchannels," J. Electron. Mater., **18**(5), pp. 611–617.
[3] Xie, X. L., Liu, Z. J., He, Y. L., and Tao, W. Q., 2009, "Numerical Study of Laminar Heat Transfer and Pressure Drop Characteristics in a Water-Cooled Minichannel Heat Sink," Appl. Therm. Eng., **29**(1), pp. 64–74.
[4] Wan, Z. M., Guo, G. Q., Su, K. L., Tu, Z. K., and Liu, W., 2012, "Experimental Analysis of Flow and Heat Transfer in a Miniature Porous Heat Sink for High Heat Flux Application," Int. J. Heat Mass Transfer, **55**(15–16), pp. 4437–4441.
[5] Persoons, T., Saenen, T., Van Oevelen, T., and Baelmans, M., 2012, "Effect of Flow Pulsation on the Heat Transfer Performance of a Minichannel Heat Sink," ASME J. Heat Transfer, **134**(9), p. 091702.
[6] Guo, J., Yan, Y. X., Liu, W., Jiang, F. M., and Fan, A. W., 2013, "Effects of Upwind Area of Tube Inserts on Heat Transfer and Flow Resistance Characteristics of Turbulent Flow," Exp. Therm. Fluid Sci., **48**, pp. 147–155.
[7] Zhang, X. Y., Liu, Z. C., and Liu, W., 2013, "Numerical Studies on Heat Transfer and Friction Factor Characteristics of a Tube Fitted With Helical Screw-Tape Without Core-Rod Inserts," Int. J. Heat Mass Transfer, **60**, pp. 490–498.
[8] Li, P. X., Liu, Z. C., Liu, W., and Chen, G., 2015, "Numerical Study on Heat Transfer Enhancement Characteristics of Tube Inserted With Centrally Hollow Narrow Twisted Tapes," Int. J. Heat Mass Transfer, **88**, pp. 481–491.
[9] Mahmood, G. I., Simonson, C. J., and Besant, R. W., 2015, "Experimental Pressure Drop and Heat Transfer in a Rectangular Channel With a Sinusoidal Porous Screen," ASME J. Heat Transfer, **137**(4), p. 042601.
[10] Ruiz, M., and Carey, V. P., 2015, "Experimental Study of Single Phase Heat Transfer and Pressure Loss in a Spiraling Radial Inflow Microchannel Heat Sink," ASME J. Heat Transfer, **137**(7), p. 071702.
[11] Webb, R. L., 1981, "Performance Evaluation Criteria for Use of Enhanced Heat Transfer Surfaces in Heat Exchanger Design," Int. J. Heat Mass Transfer, **24**(4), pp. 715–726.
[12] Yun, J. Y., and Lee, K. S., 2000, "Influence of Design Parameters on the Heat Transfer and Flow Friction Characteristics of the Heat Exchanger With Slit Fins," Int. J. Heat Mass Transfer, **43**(14), pp. 2529–2539.
[13] Sreepathi, B. K., and Rangaiah, G. P., 2015, "Retrofitting of Heat Exchanger Networks Involving Streams With Variable Heat Capacity: Application of Single and Multi-Objective Optimization," Appl. Therm. Eng., **75**, pp. 677–684.
[14] Long, R., Li, B. D., Liu, Z. C., and Liu, W., 2015, "Multi-Objective Optimization of a Continuous Thermally Regenerative Electrochemical Cycle for Waste Heat Recovery," Energy, **93**(Pt. 1), pp. 1022–1029.
[15] Ge, Y., Liu, Z. C., and Liu, W., 2016, "Multi-Objective Genetic Optimization of the Heat Transfer for Tube Inserted With Porous Media," Int. J. Heat Mass Transfer, **101**, pp. 981–987.
[16] Copiello, D., and Fabbri, G., 2009, "Multi-Objective Genetic Optimization of the Heat Transfer From Longitudinal Wavy Fins," Int. J. Heat Mass Transfer, **52**(5–6), pp. 1167–1176.
[17] Husain, A., and Kim, K. Y., 2010, "Enhanced Multi-Objective Optimization of a Microchannel Heat Sink Through Evolutionary Algorithm

Coupled With Multiple Surrogate Models," Appl. Therm. Eng., **30**(13), pp. 1683–1691.
[18] Abdoli, A., and Dulikravich, G. S., 2014, "Multi-Objective Design Optimization of Branching, Multifloor, Counterflow Microheat Exchangers," ASME J. Heat Transfer, **136**(10), p. 101801.
[19] Ge, Y., Liu, Z. C., Liu, W., and Chen, G., 2015, "Active Optimization Design Theory and Method for Heat Transfer Unit and Its Application on Shape Design of Cylinder in Convective Heat Transfer," Int. J. Heat Mass Transfer, **90**, pp. 702–709.
[20] Hwang, C. L., and Yoon, K., 1981, *Multiple Attribute Decision Making: Methods and Applications*, Springer, Berlin.
[21] Patankar, S., 1980, *Numerical Heat Transfer and Fluid Flow*, Hemisphere Publishing, New York.
[22] Tao, W. Q., 2001, *Numerical Heat Transfer*, Xi'an Jiaotong University Press, Xi'an, China.
[23] Deb, K., Pratap, A., Agarwal, S., and Meyarivan, T., 2002, "A Fast and Elitist Multiobjective Genetic Algorithm: NSGA-II," IEEE Trans. Evol. Comput., **6**(2), pp. 182–197.